

## Supporting Information

### **Cu<sub>2</sub>O-Ag Tandem Catalysts for Selective Electrochemical Reduction of CO<sub>2</sub> to C<sub>2</sub> Products**

**Di Niu**<sup>1</sup>, **Cong Wei**<sup>1</sup>, **Zheng Lu**<sup>1</sup>, **Yanyan Fang**<sup>1</sup>, **Bo Liu**<sup>1</sup>, **Da Sun**<sup>1</sup>, **Xiaobin Hao**<sup>1,\*</sup>, **Hongge Pan**<sup>2,3</sup>  
and **Gongming Wang**<sup>1,\*</sup>

<sup>1</sup> Department of Applied Chemistry, University of Science and Technology of China, Hefei 230026, China; niudi@mail.ustc.edu.cn (D.N.); weicong@mail.ustc.edu.cn (C.W.); luzh2018@mail.ustc.edu.cn (Z.L.); fr1478@mail.ustc.edu.cn (Y.F.); liubo123@mail.ustc.edu.cn (B.L.); sunda727@mail.ustc.edu.cn (D.S.)

<sup>2</sup> Institute of Science and Technology for New Energy, Xi'an Technological University, Xi'an 710021, China; honggepan@zju.edu.cn (H.P.)

<sup>3</sup> School of Materials Science and Engineering, State Key Laboratory of Silicon Materials, Zhejiang University, Hangzhou 310027, China

\* Correspondence: haoxb@ustc.edu.cn (X.H.); wanggm@ustc.edu.cn (G.W.); Tel: +86-551-63601051 (G.W.)

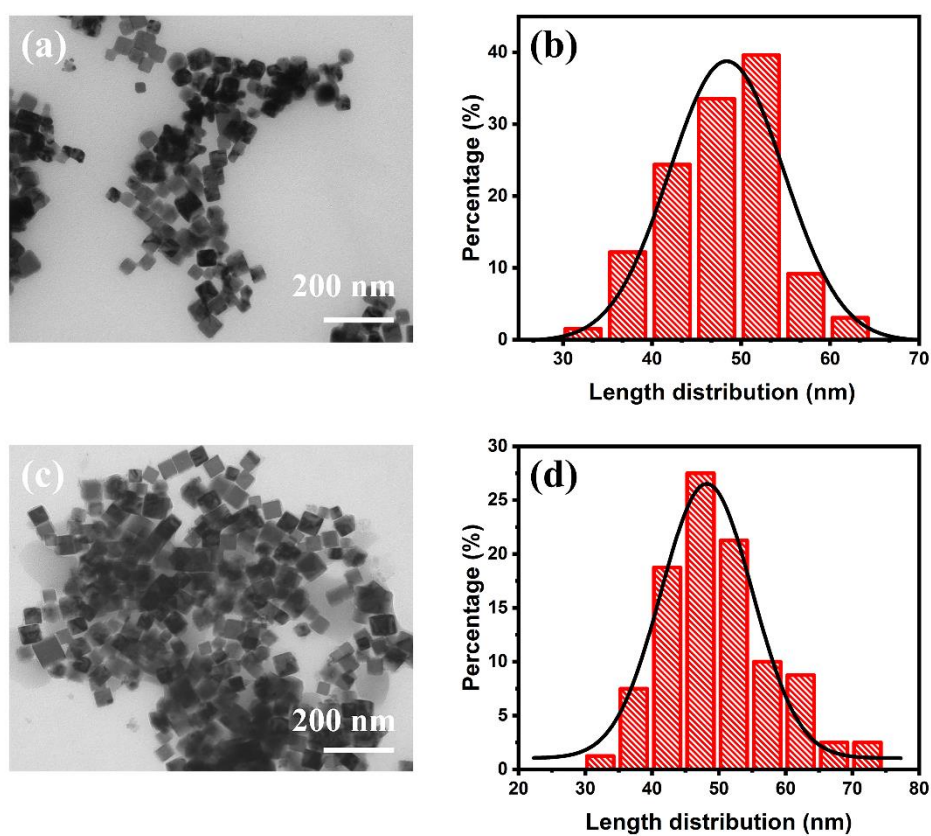


**Figure S1.** (a) TEM image and (b) size distribution of Cu<sub>2</sub>O-Ag nanocubes. (c) TEM image and (d) size distribution of Cu<sub>2</sub>O nanocubes.

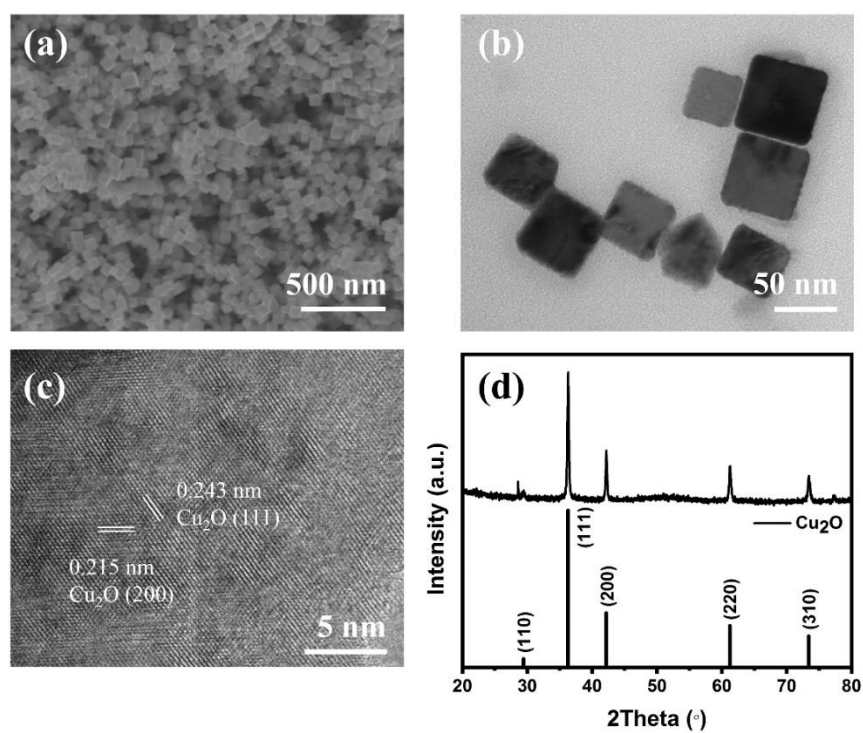


**Figure S2.** (a) SEM image of Cu<sub>2</sub>O nanocubes. (b) TEM image of Cu<sub>2</sub>O nanocubes. (c) HRTEM image of Cu<sub>2</sub>O nanocubes. (d) XRD pattern of Cu<sub>2</sub>O nanocubes.

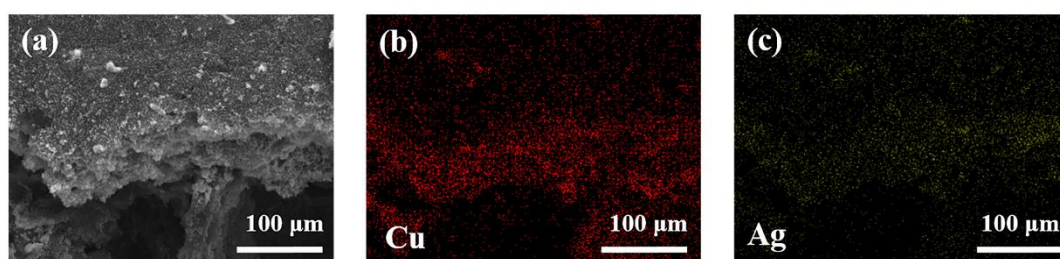


**Figure S3.** (a–c) SEM-EDS elemental mapping of Cu<sub>2</sub>O-Ag nanocubes, showing the distribution of elemental (b) Cu and (c) Ag within the particles.

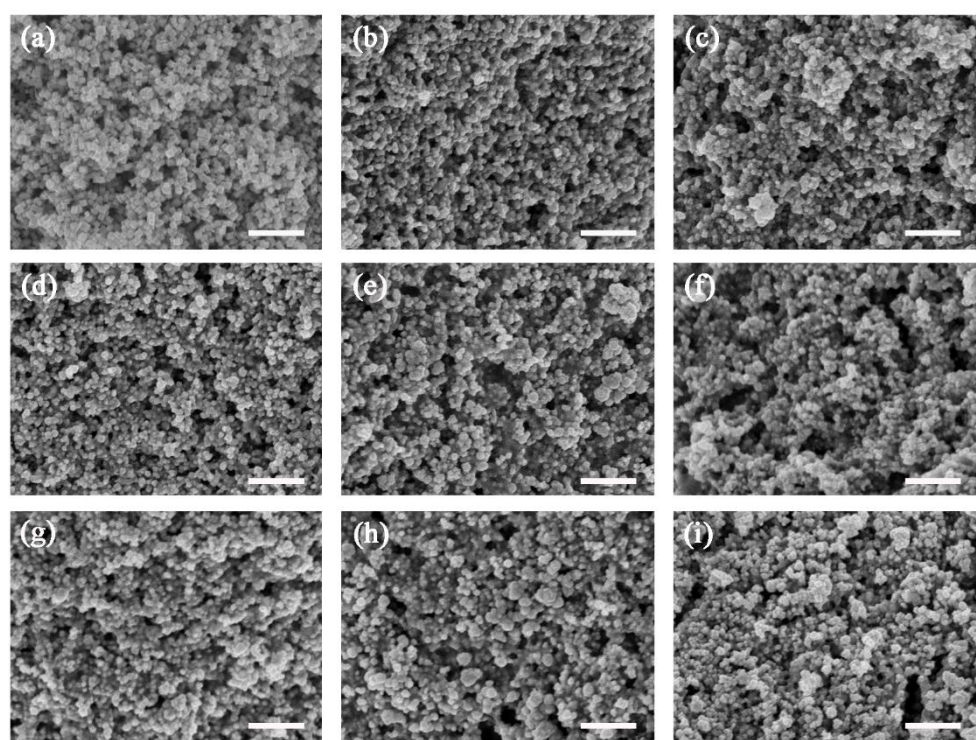


**Figure S4.** The SEM images of the Cu<sub>2</sub>O-Ag during CO<sub>2</sub>RR. (a) 0 min, (b) 5 min, (c) 10 min, (d) 15 min, (e) 20 min, (f) 25 min, (g) 30 min, (h) 35 min, (i) 40 min. Scale bar=500 nm.

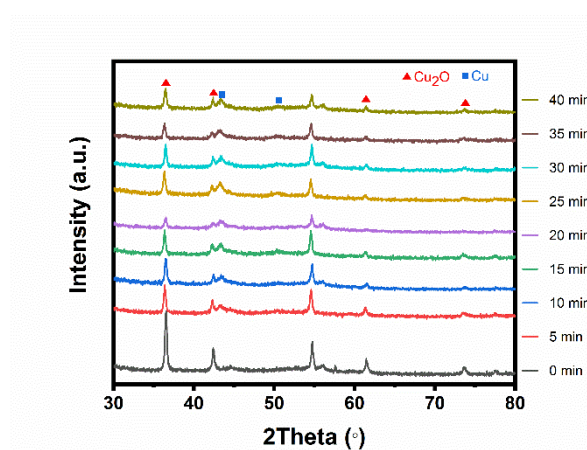


**Figure S5.** The XRD patterns of the Cu<sub>2</sub>O-Ag during CO<sub>2</sub>RR.

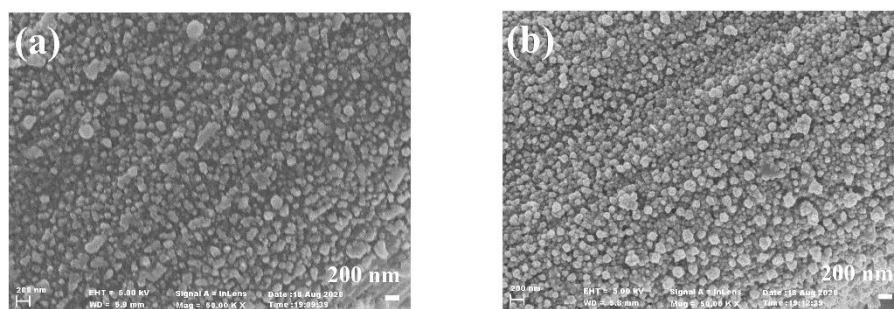


Figure S6. SEM images of (a) Cu<sub>2</sub>O-Ag nanocubes and (b) Cu<sub>2</sub>O nanocubes after CO<sub>2</sub>RR.

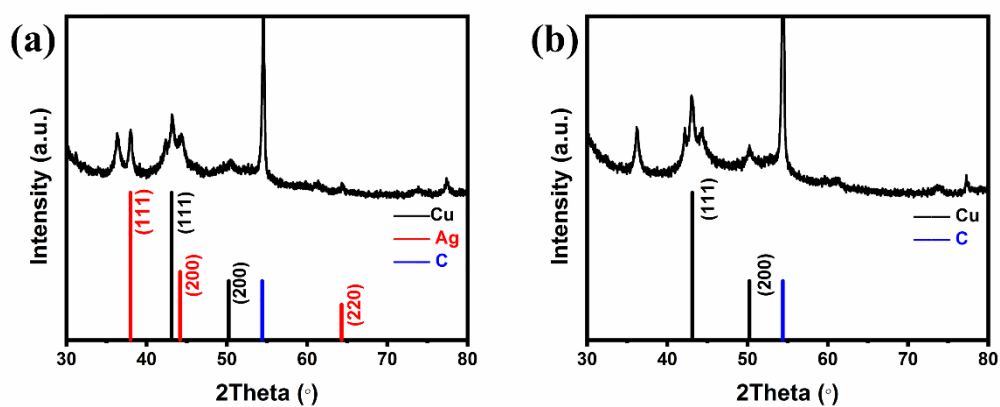


Figure S7. XRD patterns of (a) Cu<sub>2</sub>O-Ag nanocubes and (b) Cu<sub>2</sub>O nanocubes after CO<sub>2</sub>RR.

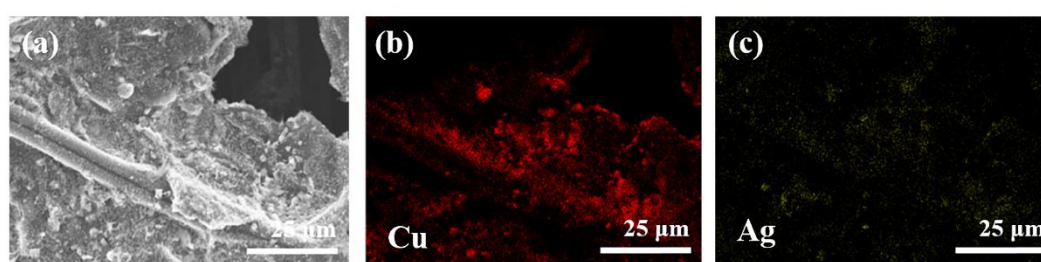


Figure S8. (a–c) SEM-EDS elemental mapping of Cu<sub>2</sub>O-Ag nanocubes of (b) Cu and (c) Ag after CO<sub>2</sub>RR.

Table S1. Cu and Ag contents of Cu<sub>2</sub>O-Ag nanocubes before and after CO<sub>2</sub>RR.

Element Content	Cu	Ag
Before CO <sub>2</sub> RR	90.28%	9.72%
After CO <sub>2</sub> RR	92.61%	7.39%

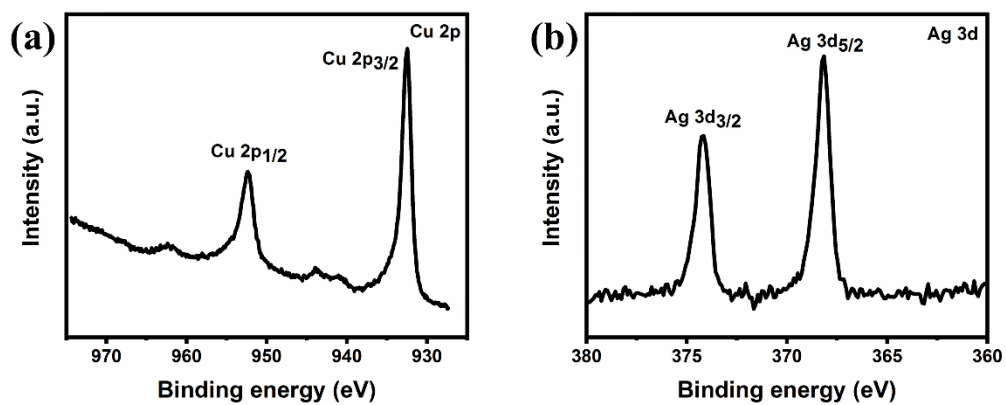


Figure S9. XPS spectra for (a) Cu and (b) Ag of Cu<sub>2</sub>O-Ag nanocubes after CO<sub>2</sub>RR.

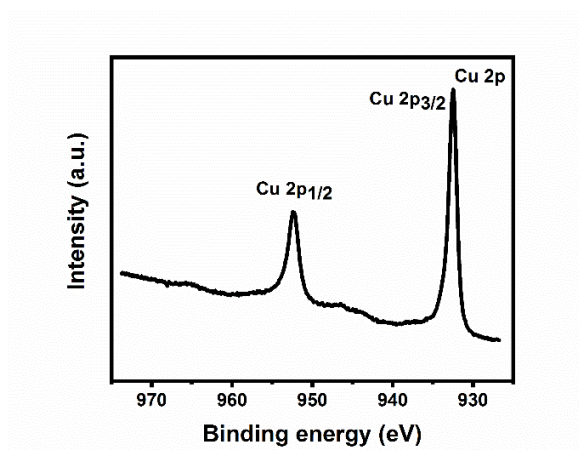


Figure S10. XPS spectra for Cu of Cu<sub>2</sub>O nanocubes after CO<sub>2</sub>RR.

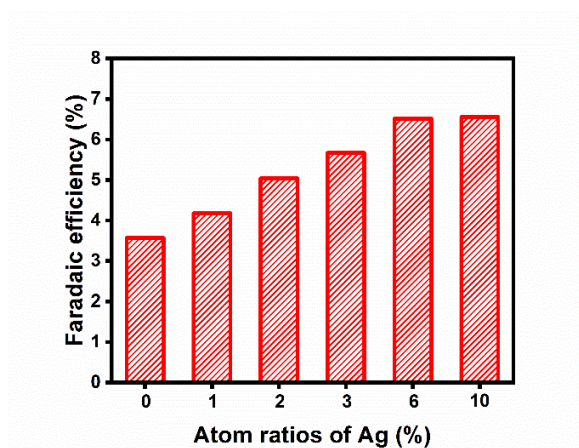
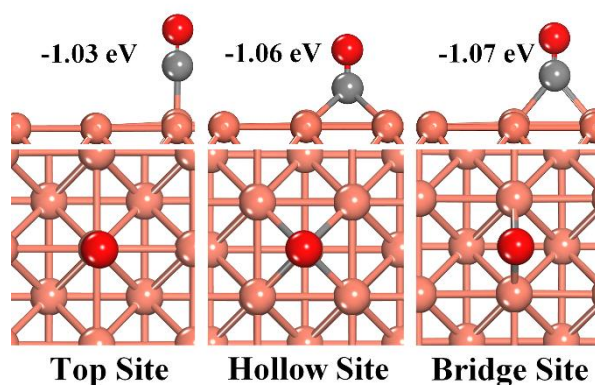
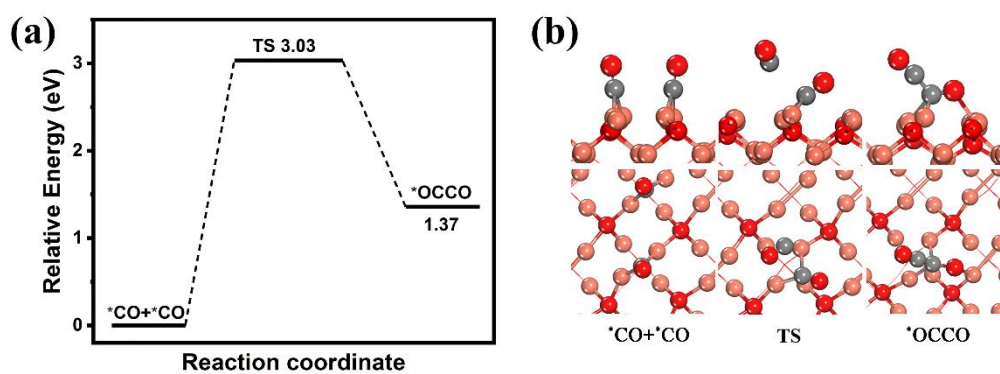


Figure S11. Faradaic efficiency of acetate of the different mass ratios of Ag in the Cu<sub>2</sub>O-Ag nanocubes.



**Figure S12.** Adsorption energy and corresponding configuration of CO at three type sites on Cu(100) surface.



**Figure S13.** (a) Reaction energy barrier diagram of the C-C coupling step on the Cu<sub>2</sub>O(100) surface with the (b) corresponding configurations of two \*CO forming an \*OCCO. Light red, copper; grey, carbon; red, oxygen; TS, transition state.